Light scattering from nematic droplets: Anomalous-diffraction approach

S. Žumer*
Liquid Crystal Institute, Kent State University, Kent, Ohio 44242
(Received 10 August 1987)

The scattering matrix, differential cross section, and total cross section for supramicrometer-size nematic droplets in a polymeric matrix are derived in the anomalous-diffraction approach. Scattering patterns are calculated in detail for three different nematic-director configurations: one characteristic of a droplet in a strong external field, the other characteristic of a droplet outside the field in the case of normal surface anchoring, and the third characteristic of an isotropic droplet with a surface-induced nematic layer. The results, which are presented graphically, indicate strong dependence of the diffraction patterns on wavelength and droplet structure. The possibilities of determining droplet size and nematic-director structure from experimental light scattering data are discussed. Special attention is paid to the possibility of the detection of the surface-induced nematic ordering.

I. INTRODUCTION

There are no exact solutions[1,2] for the light scattering from small, optically anisotropic objects. Most of the studies are devoted to very small objects such as macromolecules[1,3] or to cases where the symmetry of the dielectric tensor coincides with the symmetry of the object.[4–7] This treatment is limited to optically soft (weakly refracting) objects, where two relatively simple approximations cover the whole range of sizes: the Rayleigh-Gans approximation[8,9] (RGA) for objects smaller than the wavelength of light and of the anomalous-diffraction approach[10,11] (ADA) for larger objects.

Polymeric dispersions of liquid crystals have recently been developed for use in optical and optoelectronic devices.[12,13] These materials consist of randomly distributed micrometer-size nematic droplets embedded in an isotropic solid polymer. The size of spherical droplets is usually uniform throughout the dispersion but can vary between 0.1 and 10 μm. The nematic-director configuration within droplets depends on surface anchoring, elastic constants, and external field. Droplets are optically anisotropic objects with the direction of the optical axis varying in space according to the local nematic director.[11,13] In most cases, the two principal indices of refraction of the nematic liquid crystal range between 1.5 and 1.75, differing only slightly from the surrounding polymer ($n_m \sim 1.55$). Therefore, nematic droplets in a polymeric matrix can always be treated as optically soft objects. The first paper[14] on this subject treated scattering within RGA; therefore, the results were limited to relatively small droplets. The following discussion presents a continuation of this study. The anomalous-diffraction approach will encompass situations where droplets are larger than the wavelength of light. The goal of this study is the analysis of the possible use of light scattering for droplet structure characterization. Such a determination would contribute to the basic understanding of the effect of confinement on the nematic phase and of surface-induced nematic ordering in the isotropic phases.[15–20] Until now, the N-I (nematic-isotropic) phase transition and the surface N-I transition have been studied only in planar geometry, which is experimentally very demanding. The second important reason for this study is the controllability of the nematic structures by the external field or temperature which is of great importance for optoelectronic applications.[12,13]

Section II introduces the differential and total cross sections and relates them to the scattering matrix. Section III develops ADA, taking into account birefringence of the scattering objects. Section IV treats light scattering from three simple director configurations in detail: (A) strongly oriented structure, (B) radial structure, and (C) isotropic droplet with surface-induced nematic layer. Numerical results for scattering patterns and cross sections are presented in Sec. V. The possibility for determining droplet size and nematic-director structure from a comparison with experimental data is discussed.

II. SCATTERING CROSS SECTIONS

The amount and distribution of the scattered light from a single object is usually described by the corresponding total and differential cross sections. To introduce these quantities, we start with an incoming plane wave with the corresponding wave vector **k**,

$$\mathbf{E}=\mathbf{E}_0 e^{i\mathbf{k}\cdot\mathbf{r}+i\omega t} , \tag{1}$$

and a scattered wave which can, in a far-field regime, be described by an angularly modulated spherical wave,[14]

$$\mathbf{E}_S=\mathbf{f}(\mathbf{k},\mathbf{k}')\frac{e^{-ikr}}{r} . \tag{2}$$

Here $\mathbf{f}(\mathbf{k},\mathbf{k}')$ stands for the scattering amplitude and $\mathbf{k}'$ with $|\mathbf{k}'|=|\mathbf{k}|$ for the scattering wave vector. Introducing the van Hulst scattering matrix $\underline{S}$ one can write

$$\mathbf{E}_S=\underline{S}\mathbf{E}_0\frac{e^{-ikr}}{ikr} , \tag{3}$$

where

$$\mathbf{f}=E_0\underline{S}\mathbf{e}/ik \quad \text{with } \mathbf{e}=\frac{\mathbf{E}_0}{E_0} . \tag{4}$$

In respect to a chosen scattering plane given by $\mathbf{k}$ and $\mathbf{k}'$, it is convenient to divide $\mathbf{E}_0$ and $\mathbf{E}_S$ into components $\mathbf{E}_{0\parallel}$ and $\mathbf{E}_{S\parallel}$, parallel to the scattering plane, and to components $E_{0\perp}$ and $E_{S\perp}$, orthogonal to the scattering plane (see Fig. 1). We can rewrite Eq. (3) as

$$\begin{bmatrix} E_{S\parallel} \\ E_{S\perp} \end{bmatrix} = \begin{bmatrix} S_{\parallel\parallel} & S_{\parallel\perp} \\ S_{\perp\parallel} & S_{\perp\perp} \end{bmatrix} \begin{bmatrix} E_{0\parallel} \\ E_{0\perp} \end{bmatrix} \frac{e^{-ikr}}{ikr} . \tag{5}$$

The distribution of the scattered light can now be represented by a differential cross section,

$$\frac{d\sigma}{d\Omega}=\left|\frac{\mathbf{E}_S}{E_0}\right|^2 r^2=\left|\frac{\mathbf{f}}{E_0}\right|^2=\frac{1}{k^2}|\underline{S}\mathbf{e}|^2 . \tag{6}$$

With the previous separation into $\parallel$ and $\perp$ components, Eq. (6) can be written as

$$\left.\begin{matrix}(d\sigma/d\Omega)_\parallel \\ (d\sigma/d\Omega)_\perp\end{matrix}\right\} = \frac{1}{k^2}\left\{\begin{matrix}|S_{\parallel\parallel}\cos\alpha+S_{\parallel\perp}\sin\alpha|^2 \\ |S_{\perp\parallel}\cos\alpha+S_{\perp\perp}\sin\alpha|^2 ,\end{matrix}\right. \tag{7}$$

where α is the angle between the polarization vector $\mathbf{e}$ and the scattering plane. The total cross section

$$\sigma_S=\int\frac{d\sigma}{d\Omega}d\Omega \tag{8}$$

is then given by

$$\sigma_S=\frac{1}{k^2}\int[\,|S_{\parallel\parallel}(\mathbf{i}_\parallel\cdot\mathbf{e})+S_{\parallel\perp}(\mathbf{i}_\perp\cdot\mathbf{e})|^2 + |S_{\perp\parallel}(\mathbf{i}_\parallel\cdot\mathbf{e})+S_{\perp\perp}(\mathbf{i}_\perp\cdot\mathbf{e})|^2]d\Omega , \tag{9}$$

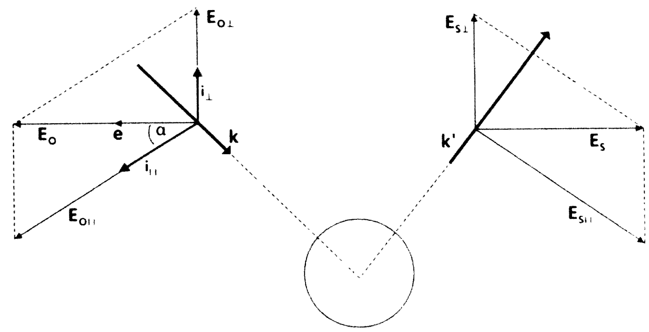

FIG. 1. Schematic representation of the separation of the electric field of the incident and scattered light into parallel ($\parallel$) and orthogonal ($\perp$) components with respect to the scattering plane.

where $\mathbf{i}_\perp$ and $\mathbf{i}_\parallel$ are unit vectors orthogonal to the direction of the incoming wave vector, perpendicular and parallel to the scattering plane, respectively (see Fig. 1). This integral need not be calculated because one can use the well-known optical theorem,[11,21]

$$\sigma_S=\frac{4\pi}{k}E_0\,\mathrm{Im}[\mathbf{e}\cdot\mathbf{f}(\mathbf{k},\mathbf{k}'=\mathbf{k})] , \tag{10}$$

which, using the scattering matrix, can be written as

$$\sigma_S=\frac{4\pi}{k^2}\mathrm{Re}[\mathbf{e}\cdot\underline{S}(\mathbf{k},\mathbf{k}'=\mathbf{k})\mathbf{e}] , \tag{11}$$

or more explicitly,

$$\sigma_S=\frac{4\pi}{k^2}\mathrm{Re}\{(\mathbf{i}_\parallel\cdot\mathbf{e})^2S_{\parallel\parallel}(o)+(\mathbf{i}_\parallel\cdot\mathbf{e})(\mathbf{i}_\perp\cdot\mathbf{e})[S_{\parallel\perp}(o)+S_{\perp\parallel}(o)]+(\mathbf{i}_\perp\cdot\mathbf{e})^2S_{\perp\perp}(o)\} . \tag{12}$$

Here argument (o) stands for $\mathbf{k}'=\mathbf{k}$. Comparing Eqs. (2) and (11) one can test calculations of $\underline{S}$. It is worthwhile to stress that for $\mathbf{k}'=\mathbf{k}$ the scattering plane is no longer defined. Therefore any convenient frame can be chosen as a reference for vectors $\mathbf{i}_\perp$ and $\mathbf{i}_\parallel$ and matrix $\underline{S}$.

III. ANOMALOUS-DIFFRACTION APPROACH

According to van de Hulst,[11] the anomalous diffraction (AD) limit is reached when conditions $kR \gg 1$ and $n_r-1 \ll 1$ are realized. Here n_r stands for the relative index of refraction of the scattering object and R is its typical size (for a sphere, R is just the radius). The first condition ($kR \gg 1$) allows the ray picture of the light propagation. The second condition allows the neglect of reflections on external and internal boundaries and the refraction of the ray passing the scattering object. Therefore in the AD approximation a scattering object does not change either the direction of the propagation or the amount of light but only introduces a phase shift Δ depending on the direction of the ray. The difference in the directions of the field vectors $\mathbf{E}$ and $\mathbf{D}$ in the droplet is neglected as well. Far-field distribution of the scattered light can be, in such a case, calculated in a way that is similar to the Fraunhofer diffraction pattern. There are two contributions to the scattered field: (1) light scattered by an opaque object which, according to the Babinet principle,[21] is equal to the field scattered by a conjugated screen [here a three-dimensional (3D) object is approximated by a planar screen] but for a Π-phase shift, and (2) light transmitted and phase-shifted by the scattering object.

For an isotropic object or an object with uniformly oriented local principal axes $\mathbf{n}$ (nematic director in the case of a nematic droplet), where $\mathbf{E}_0$ is either in the plane of incidence (defined by vectors $\mathbf{k},\mathbf{n}$) or orthogonal to it, the scattered field is simply given by[14]

$$\mathbf{E}_S=\mathbf{E}_0\frac{k^2}{2\pi}\int\frac{e^{i\mathbf{k}'\cdot(\mathbf{r}+\mathbf{r}'')}}{i\mathbf{k}'\cdot(\mathbf{r}+\mathbf{r}'')}(1-e^{i\Delta(\mathbf{r}'')})dA . \tag{13}$$

Here the integral goes over the area A covered by a pro-

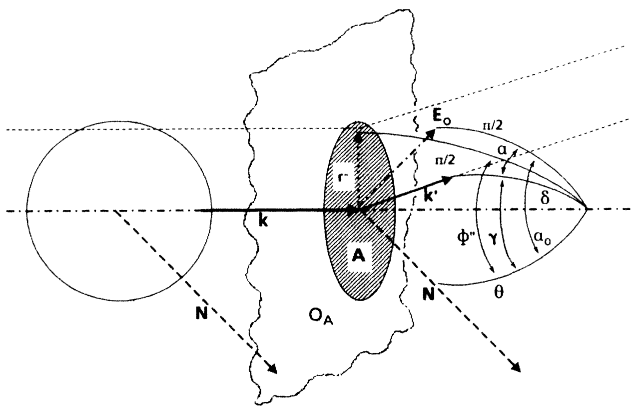

FIG. 2. Schematic presentation of the droplet projection to the O_A plane which is perpendicular to vector **k**. Vectors **k**′, **r**″, $\mathbf{E}_0$, and **N** (droplet director) with corresponding angles are shown as well.

jection of the object on the plane O_A, orthogonal to the wave vector **k** (see Fig. 2). Vectors **k**′, **r**, and **r**″ are defined on the figure. The phase shift $\Delta(\mathbf{r}'')$ of a ray passing the plane O_A at **r**″ depends on the droplet size and shape and on the orientation of the principal axis.

To describe the general situation where the direction of the optical axis **n** and the principal values of the index of refraction n_0 and n_e depend on the position in the object, we modify Eq. (13) to

$$\mathbf{E}_S=\frac{k^2}{2\pi}\int[1-\underline{P}(\mathbf{r}'')]\frac{e^{i\mathbf{k}'\cdot(\mathbf{r}+\mathbf{r}'')}}{i\mathbf{k}'\cdot(\mathbf{r}+\mathbf{r}'')}dA\,\mathbf{E}_0\,. \tag{14}$$

Here matrix $\underline{P}(\mathbf{r}'')$ describes the induced phase shift and the rotation of the polarization vector for a ray passing the plane O_A at point **r**″. Usually $\underline{P}$ must be calculated numerically for a given object.

As we are looking for the far-field (Fraunhofer) diffraction we can approximate $(\mathbf{r}+\mathbf{r}'')$ in the denominator by **r** and rewrite Eq. (14) in the following form:

$$\mathbf{E}_S=\frac{e^{ikr}}{ikr}\frac{k^2}{2\pi}\int[1-\underline{P}(\mathbf{r}'')]e^{i\mathbf{k}'\cdot\mathbf{r}''}dA\,\mathbf{E}_0\,, \tag{15}$$

and further comparing it to Eq. (3), find the expression for the scattering matrix,

$$\underline{S}=\frac{k^2}{2\pi}\int(1-\underline{P})e^{i\mathbf{k}'\cdot\mathbf{r}''}dA\,. \tag{16}$$

We introduce angular coordinates δ and γ to specify the direction of the scattered wave vector **k**′ with respect to the incoming vector **k** and some chosen reference coordinate system. This system is usually attached to the symmetry axis of the object (droplet director **N**; see Fig. 2). Further, we introduce the angle Φ'' between **r**″ and the interception line of the plane defined by vectors **k** and **N** and the O_A plane, so that we can write

$$\mathbf{k}'\cdot\mathbf{r}''=kr''\cos(\gamma-\Phi'')\sin\delta\,. \tag{17}$$

Expressing the surface element dA with $d\Phi''r''dr''$ we finally get

$$\underline{S}=\frac{k^2}{2\pi}\int(1-\underline{P})e^{ikr''\cos(\gamma-\Phi'')\sin\delta}d\Phi''r''dr''\,, \tag{18}$$

where $\underline{P}$ is a function of k, γ, θ (the angle between **k** and **N**), Φ'', and of object shape, size, and structure. In general, it cannot be calculated analytically. The total cross section defined by Eq. (11) then becomes

$$\sigma_S=2\int[1-\mathbf{e}\cdot(\mathrm{Re}\underline{P})\mathbf{e}]d\Phi''r''dr''\,. \tag{19}$$

In the following we will treat some examples where nematic-director configuration within a spherical droplet can be easily calculated.

IV. SCATTERING FROM SOME SIMPLE DIRECTOR CONFIGURATIONS

A nematic liquid crystal confined to a small volume exhibits a specific nematic-director configuration[22,14,23] which depends on elastic forces, surface interactions, and possible external field. In supramicrometer-size droplets, surface-induced changes in the value and anisotropy of the nematic order parameter can be neglected,[24,25] except in the vicinity of the nematic-isotropic transition. Also, we neglect a possible influence of the external field on the order parameter.[26] Therefore, if not stated additionally a constant nematic order-parameter approximation will be used. Assuming strong molecular anchoring on the droplet surface, the nematic-director configuration **n** is obtained after a minimization of the elastic and electric (if the field is present) free energy.[27] In cases with cylindrical symmetry one can, in a single elastic constant approximation ($K_{11}=K_{22}=K_{33}=K$), find the partial differential equation

$$\nabla^2\theta_n-\left[\frac{1}{\xi^2}+\frac{1}{\rho^2}\right]\cos\theta_n\sin\theta_n=0 \tag{20}$$

for the angle θ_n between the local director **n** and the direction of the symmetry axis **N** (droplet director). Here ρ is the cylindrical coordinate and ξ is the correlation length[27] of the orientational order induced by an infinitely strong planar surface anchoring in the bulk nematic if the external field is not parallel to the surface preferred direction. In the case of an electric field E (for an insulator regime[27]) we have

$$\xi=\left[\frac{K}{\Delta\epsilon\epsilon_0}\right]^{1/2}\frac{1}{E}\,, \tag{21}$$

where $\Delta\epsilon$ stands for low-frequency anisotropy of the liquid crystalline dielectric constant. For $K\sim5\times10^{-12}$ N, $\Delta\epsilon=0.5$, and $E=1$ V/μm, one finds $\xi\simeq1\ \mu$m.

Solutions of nonlinear partial differential Eq. (20) can be obtained using the well-known numerical over relaxation method.[28] In the following we are going to treat scattering from three simple structures.

A. Uniformly oriented spherical nematic droplet

The situation shown schematically in Fig. 3 can be realized in a very strong external electric or magnetic field ($\xi<<R$). The local director **n** is parallel practically everywhere to the droplet director **N**. In this case, the thin boundary layer will be neglected. In such a case, the droplet polarization vectors of the ordinary and extraor-

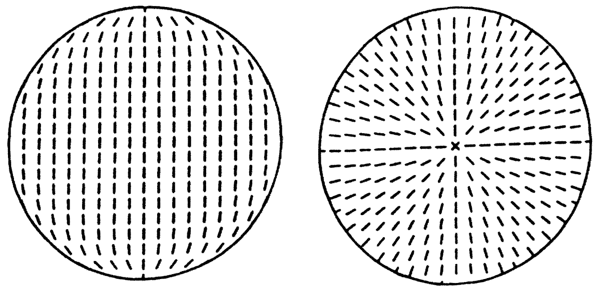

FIG. 3. Schematic presentation of the director configuration in the oriented droplet (a) and in the droplet with radial structure (b).

dinary ray do not rotate. Let us first consider the situation when the plane of incidence (defined by **k** and **N**) is also the scattering plane ($\gamma=0$). Then $\underline{P}$ is diagonal and given by the corresponding phase shifts,

$$\underline{P}(\gamma=0)=\begin{bmatrix} e^{i\Delta_e(\theta,r'')} & 0 \\ 0 & e^{i\Delta_0(r'')} \end{bmatrix}, \tag{22}$$

where

$$\Delta_0=2k(n_0/n_m-1)(R^2-r''^2)^{1/2} \tag{23a}$$

and

$$\Delta_e=2k[n_e(\theta)/n_m-1](R^2-r''^2)^{1/2}, \tag{23b}$$

with

$$n_e(\theta)=\left[\frac{\cos^2\theta}{n_0^2}+\frac{\sin^2\theta}{n_e^2}\right]^{-1/2}. \tag{24}$$

Here n_m is the index of refraction of the surrounding media, n_0 and n_e are the two principal indices of the nematic liquid crystal, and θ is the angle between **k** and **N** (see Fig. 2). The scattering matrix can be written as

$$\underline{S}(\gamma=0)=k^2\int_0^R[1-\underline{P}(\gamma=0)]J_0(kr''\sin\delta)r''dr'', \tag{25}$$

where J_0 is the Bessel function of the zeroth order. The integral cannot be calculated analytically in closed form except for $\delta=0$, where one finds

$$\underline{S}(\delta=0,\gamma=0)=\frac{k^2R^2}{2}\begin{bmatrix} H\left[i2kR\left[\frac{n_e(\theta)}{n_m}-1\right],0\right] & 0 \\ 0 & H\left[i2kR\left[\frac{n_0}{n_m}-1\right],0\right] \end{bmatrix}. \tag{26}$$

Here $H(w,0)$ stands for

$$H(w,0)=1+\frac{2e^{-w}}{w}+2\frac{e^{-w}-1}{w^2}. \tag{27}$$

The total diffraction cross section then becomes

$$\sigma_S=2\pi R^2\left\{\cos^2\alpha_0 H\left[i2kR\left[\frac{n_e(\theta)}{n_m}-1\right],0\right] +\sin^2\alpha_0 H\left[i2kR\left[\frac{n_0}{n_m}-1\right],0\right]\right\}, \tag{28}$$

where α_0 is the polarization angle (see Fig. 2) and Re stands for the real part. After some rearrangement, one finds

$$\sigma_S=2\sigma_0[\cos^2\alpha_0 H'(v_e,0)+\sin^2\alpha_0 H'(v_0,0)], \tag{29}$$

where σ_0 is the geometrical cross section,

$$H'(v,0)=1-\frac{2}{v}\sin v+\frac{2}{v^2}(1-\cos v), \tag{30}$$

where v is either v_e or v_0 defined as

$$v_e=2kR\left[\frac{n_e(\theta)}{n_m}-1\right], \tag{31a}$$

and

$$v_0=2kR\left[\frac{n_0}{n_m}-1\right]. \tag{31b}$$

For numerical calculations we have chosen the following indices of refraction: $n_e=1.70$, $n_0=1.52$, and $n_m=1.55$. The resulting σ_S as functions of kR for six different incident angles θ (angle between **k** and **N**) and $\alpha=0$ (polarization in the plane of incidence) are presented in Fig. 4. In all cases, the general behavior of σ_S is the same and comparable to the isotropic case.[14] For small values of kR, the total cross section is given by

$$\sigma_S=2\sigma_0(kR)^2\left[\cos^2\alpha_0\left[\frac{n_e(\theta)}{n_m}-1\right]^2 +\sin^2\alpha_0\left[\frac{n_0}{n_m}-1\right]^2\right]. \tag{32}$$

The same expression is obtained[11] with RGA in the limit $kR>1$ if condition $2kR(n/n_m-1)\ll 1$ is satisfied, where n can be either n_e or n_0. The RGA values for σ_S are shown in Fig. 4 for comparison. For larger values of kR where

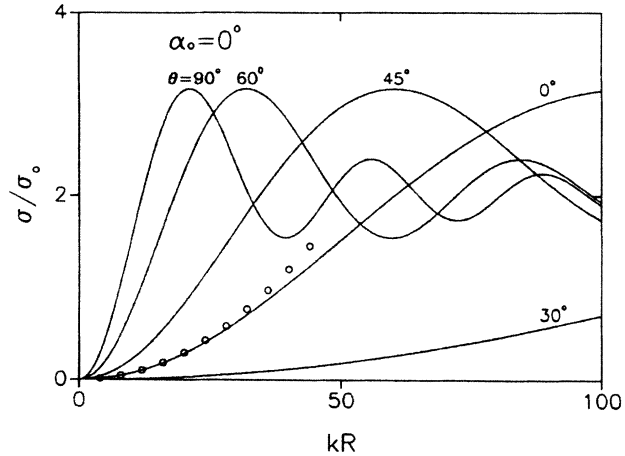

FIG. 4. The dependence of the total cross section of the oriented droplet on kR or different angles of incidence ($\theta=0°,30°,45°,60°,90°$) with $\alpha_0=0$. The RGA results for $\theta=0°$ and $\alpha_0=0$ are represented by circles.

$$kR\left|\frac{n}{n_m}-1\right|>\pi ,$$

σ_S starts to oscillate around the asymptotic value $2\sigma_0$. The wavelength of these oscillations strongly depends on θ and α_0. This behavior is the result of the constructive or destructive interference between transmitted and diffracted light. Figure 5 shows that by increasing the polarization angle α_0 from 0°, the contribution of the fast oscillating term due to the extraordinary ray decreases, and the contribution of the slow oscillating term due to the ordinary ray increases. It must be stressed that for special cases of index matching, $n_0=n_m$. There is no ordinary ray scattering; thus the limiting value of σ_S is $2\sigma_0\cos^2\alpha$ instead of $2\sigma_0$.

Figures 6(a) and 6(b) show the dependence of σ_S/σ_0 on the incident angle θ for different kR values and for (a) $n_0=1.52<n_m=1.55<n_e=1.70$, and (b) $n_0=n_m=1.52<n_e=1.70$. The polarization angle α_0 is zero for both cases. The minima $\sigma_s=0$ correspond to the matching of the extraordinary index of refraction with the index of the surrounding matrix, while the local minima at higher kR have an interference nature. It is worthwhile to notice [see Eq. (29)] that the θ dependence decreases with increasing α_0, and at $\alpha_0=90°$ it completely vanishes (ordinary ray).

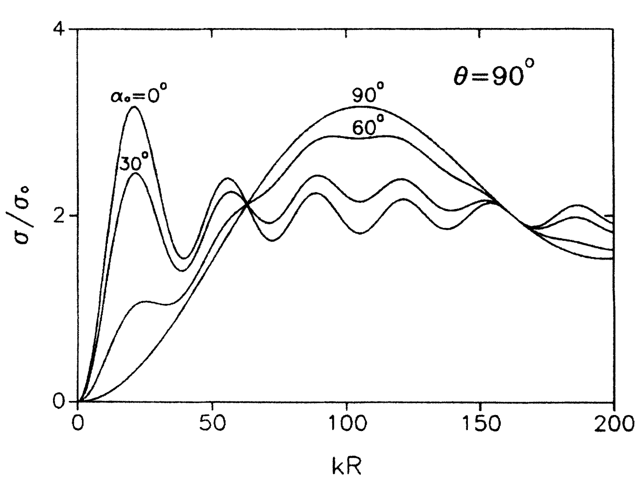

FIG. 5. The dependence of the total cross section of the oriented droplet on kR for different polarization angles $\alpha_0=0°,30°,60°,90°$ with $\theta=90°$.

To get a differential cross section one must calculate $\underline{S}$ for a general direction of the scattering vector $\mathbf{k}'(\gamma\neq0)$. In our case of uniform molecular alignment, one can get $\underline{S}(\gamma\neq0)$ with a simple rotation,

$$\underline{S}=\underline{U}(\gamma)\underline{S}(\gamma=0)\underline{U}^{-1}(\gamma) , \tag{33}$$

where

$$\underline{U}(\gamma)=\begin{vmatrix}\cos\gamma & +\sin\gamma\\ -\sin\gamma & \cos\gamma\end{vmatrix} . \tag{34}$$

The resulting scattering matrix is then

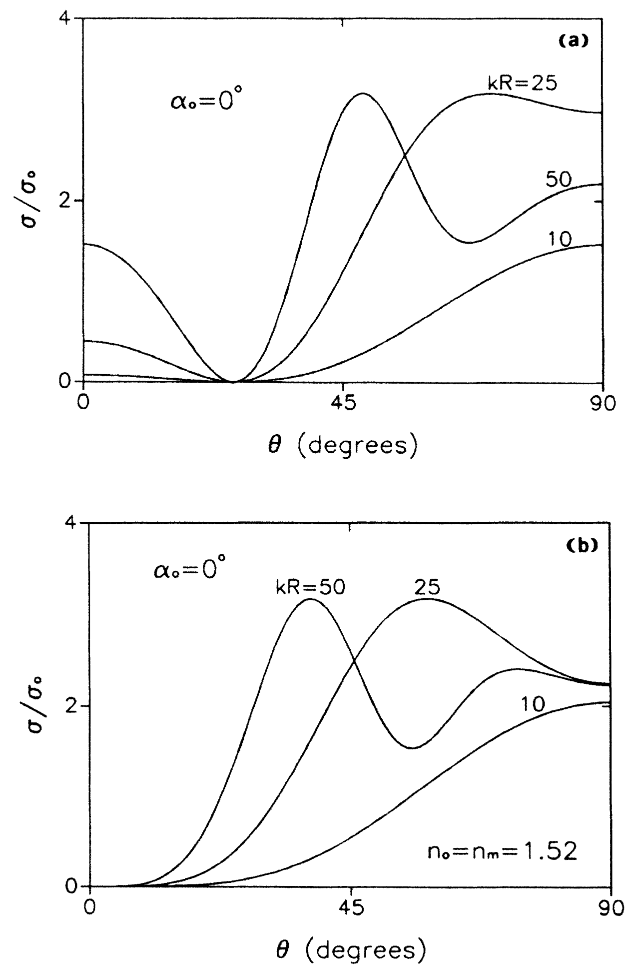

FIG. 6. The angular dependence of the total cross section of the oriented droplet for $kR=10$, 25, and 50, and for two different sets of the indices of refraction: (a) $n_0=1.52$, $n_m=1.55$, and $n_e=1.70$; and (b) $n_0=n_m=1.52$ and $n_e=1.70$.

$$\underline{S}=\tfrac{1}{2}k^2R^2\begin{bmatrix}\cos^2\gamma H(iv_0,z)+\sin^2\gamma H(iv_0,z) & [H(iv_0,z)-H(iv_e,z)]\sin\gamma\cos\gamma \\ [H(iv_0,z)-H(iv_e,z)]\sin\gamma\cos\gamma & \sin^2\gamma H(iv_e,z)+\cos^2\gamma H(iv_0,z)\end{bmatrix}, \tag{35}$$

where

$$H(iv,z)=H'(v,z)+iH''(v,z)=2\int_0^1\{1-\exp[iv(1-x^2)^{1/2}]\}J_0(xz)x\,dx\ , \tag{36a}$$

and

$$z=kR\sin\delta\ . \tag{36b}$$

Using Eq. (7) one finds

$$\left.\begin{matrix}\left[\dfrac{d\sigma}{d\Omega}\right]_{\parallel}\\ \\ \left[\dfrac{d\sigma}{d\Omega}\right]_{\perp}\end{matrix}\right\}=\frac{R^4k^2}{4}\begin{cases}[H'^2(v_e,z)+H''^2(v_e,z)]\sin^2\gamma\cos^2(\gamma+\alpha)+[H''^2(v_0,z)+H''^2(v_0,z)]\sin^2\gamma\sin^2(\gamma+\alpha)\\ -[H'(v_e,z)H'(v_0,z)+H''(v_e,z)H''(v_0,z)]\tfrac{1}{2}\sin^2\gamma\sin^2(\gamma+\alpha)\\ [H'^2(v_e,z)+H''^2(v_e,z)]\sin^2\gamma\cos^2(\gamma+\alpha)+[H''^2(v_0,z)+H''^2(v_0,z)]\cos^2\gamma\sin^2(\gamma+\alpha)\\ -[H'(v_e,z)H'(v_0,z)+H''(v_e,z)H''(v_0,z)]\tfrac{1}{2}\sin^2\gamma\sin^2(\gamma+\alpha)\ .\end{cases} \tag{37}$$

Taking into account $\gamma+\alpha=\alpha_0$ and combining both components,

$$\left[\frac{d\sigma}{d\Omega}\right]=\frac{R^4k^2}{4}[\,|H(iv_e,kR\sin\delta)|^2\cos^2(\alpha_0)+|H(iv_0,kR\sin\delta)|^2\sin^2(\alpha_0)]\ . \tag{38}$$

In Figs. 7(a) and 7(b), dependence of the differential cross section versus scattering angle δ is shown for three different kR values and two different incident angles θ. All patterns resemble the Fraunhofer diffraction pattern obtained by a circular screen.[21] They show cylindrical symmetry (no dependence on α), but their intensity strongly depends on the direction of the droplet director relative to the polarization vector. This direction is here described by angles θ and α_0. The angle θ governs the extraordinary index of refraction and in this way the phase shift of the corresponding part of light. The relative intensities of the ordinary and extraordinary ray are determined by α_0. For low kR values, the secondary- and higher-order maxima of the pattern are not as weak as in the case of the diffraction on the opaque screen.[21] Their relatively strong contribution to the total amount of scattered light is clearly shown in Fig. 8, where the amount of the light scattered within a cone defined by the scattering angle δ and given by

$$\sigma(\delta)=\int_0^{2\Pi}\int_0^{\delta}\frac{d\bar{\sigma}}{d\Omega}\sin\delta\,d\delta\,d\alpha \tag{39}$$

is shown for two kR values. For $kR=100$ and the droplet orientation $\theta=90°$, $\alpha_0=0°$, where the index of refraction is largest, droplets already behave as opaque screens. The height of the central maximum is in the limit $kR\to\infty$ proportional to $(kR)^2$ and the width is thus inversely proportional to kR.

B. Droplet with a radial structure

This situation is realized when there is no external field and the surface of a spherical cavity prefers the normal alignment of the molecules. The matrix $\underline{P}$ can be written as

$$\underline{P}=\underline{U}(\phi'')\begin{bmatrix}e^{i\Delta_e(r'')} & 0\\ 0 & e^{i\Delta_0(r'')}\end{bmatrix}\underline{U}\left[\phi''\right]^{-1}, \tag{40}$$

where $\underline{U}$ is given by Eq. (34), Δ_0 by Eq. (23a), and $\Delta_e(r'')$ by

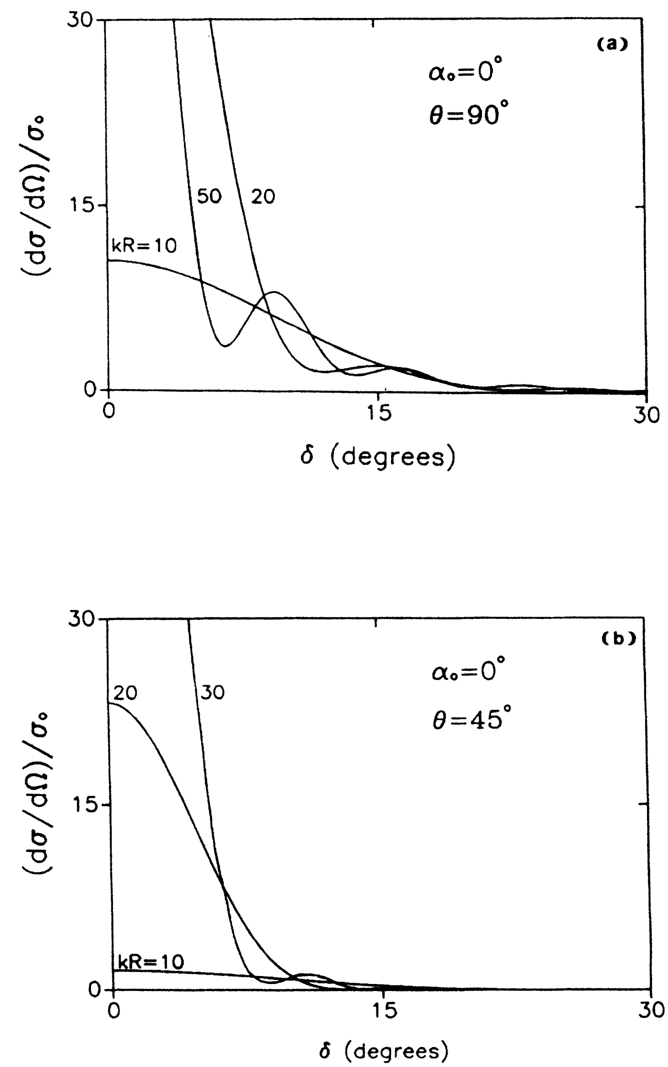

FIG. 7. The angular dependence of the differential cross section of the oriented droplet for three different kR and $\alpha_0=0$; (a) corresponds to $\theta=90°$ and (b) to $\theta=45°$.

$$\Delta_e(r'')=2k\int_0^{(R^2-r''^2)^{1/2}}\left[\frac{1}{n_m}\left[\frac{r''^2+l^2}{(r''/n_e)^2+(l/n_0)^2}\right]^{1/2}-1\right]dl\ . \tag{41a}$$

Equation (41a) can be integrated so that one has

$$\Delta_e=2kR\left[\frac{n_0}{n_m}\right]\left[yF\left\{\arctan\left[\frac{n_e}{n_0}(1-y^2)^{1/2}\right],\left[1-\left[\frac{n_0}{n_e}\right]^2\right]^{1/2}\right\}-yE\left\{\arctan\left[\frac{n_e}{n_0}(1-y^2)^{1/2}\right],\left[1-\left[\frac{n_0}{n_e}\right]^2\right]^{1/2}\right\}\right.$$
$$\left.+\left[\frac{(y^2-1)}{1-y^2[1-(n_0/n_e)^2]}\right]^{1/2}\right]-(1-y^2)^{1/2}\ , \tag{41b}$$

where y stands for r''/R, $F(u,v)$ for the generalized hypergeometric series, and $E(u,v)$ for the elliptic integral of the second kind. Putting everything together one finds

$$\underline{S}=(kR^2\int_0^1[\underline{P}-1J_0(kRy\sin\delta)]y\,dy\ , \tag{42}$$

where

$$\underline{P}=\frac{1}{2}\begin{bmatrix}B_-e^{i\Delta_e}+B_+e^{i\Delta_0} & 0\\ 0 & B_+e^{i\Delta_e}+B_-e^{i\Delta_0}\end{bmatrix} \tag{43}$$

with

$$B_\pm=[J_0(kRy\sin\delta)\pm J_2(kRy\sin\delta)]\ . \tag{44}$$

Here J_0 and J_2 are Bessel functions. The differential cross section then becomes

$$\left[\frac{d\sigma}{d\Omega}\right]=\frac{R^4k^2}{4}[(C_+^2+D_+^2)\cos^2\alpha+(C_-^2+D_-^2)\sin^2\alpha]\ , \tag{45}$$

where

$$C_\pm=\int_0^1[(J_0\mp J_2)\cos\Delta_e+(J_0\pm J_2)\cos\Delta_0-2J_0]y\,dy\ , \tag{46a}$$

and

$$D_\pm=\int_0^1[(J_0\mp J_2)\sin\Delta_e+(J_0\pm J_2)\sin\Delta_0]y\,dy\ . \tag{46b}$$

The argument for all Bessel functions is $kRy\sin\delta$. The first part of the right-hand side of Eq. (45) corresponds to $(d\sigma/d\Omega)_\parallel$ and the second to $(d\sigma/d\Omega)_\perp$. The residual integration must be performed numerically.

To get the total cross section, we start with Eq. (42) for $\delta=0$ and, inserting results for $\underline{S}$ in Eq. (12), we find

$$\sigma_S=2\sigma_0\int_0^1(2-\cos\Delta_\parallel-\cos\Delta_\perp)y\,dy\ . \tag{47}$$

For $n_e=n_0$, the result reduces to the well-known isotropic case. The total cross section as a function of kR is shown in Fig. 9. There is no polarization dependence. The irregular oscillations, similar to those of the oriented droplet for α_0 near 45°, are also caused here by the mixing of the ordinary and extraordinary ray. The large kR limiting value of σ_S/σ_0 is 2, except in the case of index matching ($n_0=n_m$), where it is 1. The behavior of the differential cross section presented in Figs. 10(a), 10(b),

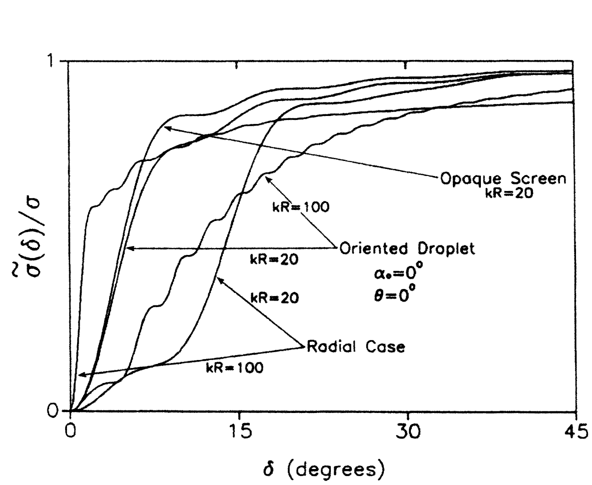

FIG. 8. The amount of the scattered light in a cone defined by the angle σ, for $kR=20$ and 100. For an opaque screen with $kR=100$, the curve coincides with an oriented case.

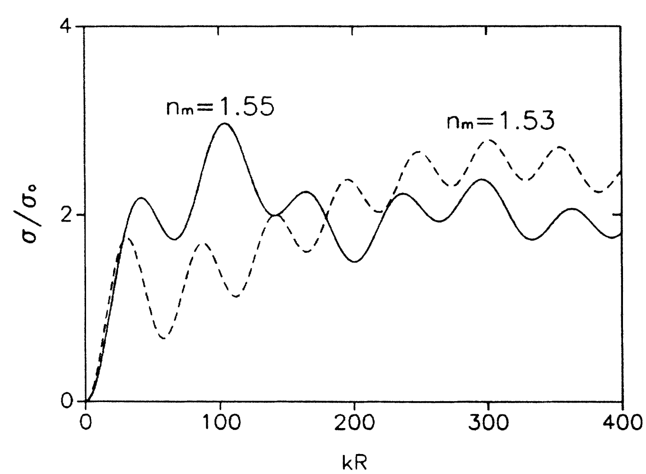

FIG. 9. The dependence of the total cross section of a droplet with radial structure on kR for $n_0=1.52$, $n_m=1.55$, and $n_e=1.70$ (solid line) and for $n_0=1.52$, $n_m=1.53$, and $n_e=1.70$ (dashed line).

11(a), and 11(b) is very different from that of oriented droplets. Diffraction patterns are anisotropic and at small kR values the secondary maximum is comparable to the central one. One can easily understand these phenomena by inspecting the phase shifts of the extraordinary and ordinary rays. For our set of indices of refraction, the phase shift of an extraordinary ray passing the center of the droplet is small. It reaches its maximum value for a ray passing the droplet projection on O_A at $\approx 0.7R$ (see Fig. 2) and then starts to decrease. The shift of the ordinary ray is maximal in the center, then it decreases and becomes zero for rays passing at R. Therefore, such a droplet effectively works as an annular screen,[21] inducing phase shifts which are larger in the direction of the polarization vector and smaller perpendicular to it. Therefore, a scattering pattern is anisotropic, depending strongly on indices of refraction and kR. At larger kR, the effect is less pronounced because the diffraction pattern is restricted to very small scattering angles. The amount of the light, $\tilde{\sigma}(\delta)$, scattered in a cone

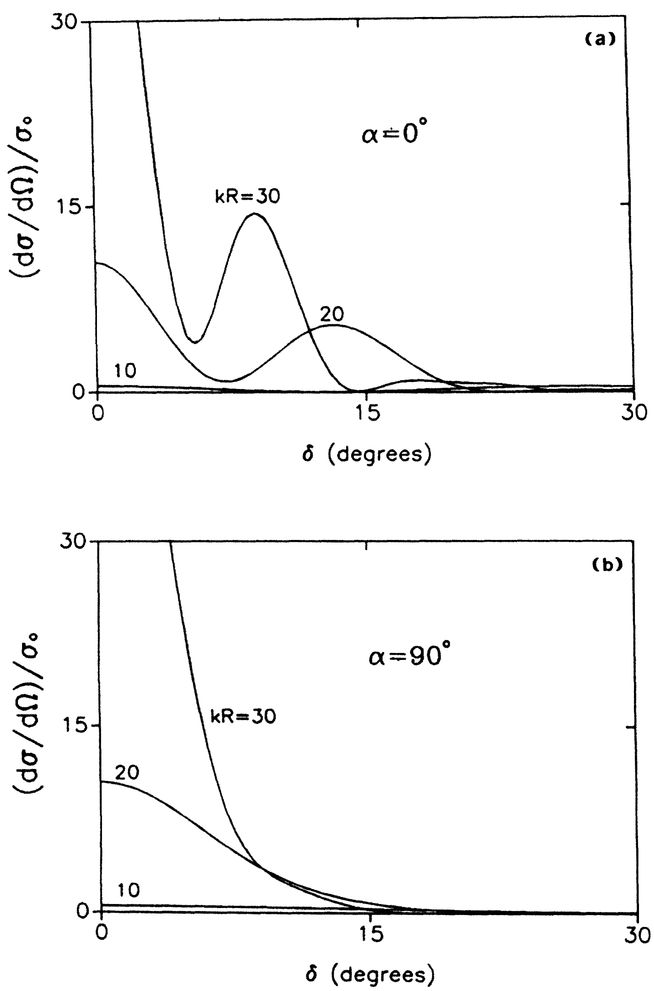

FIG. 10. The angular dependence of the differential cross section of a "radial" droplet for $kR=10$, 20, and 30 and (a) $\alpha=0°$ and (b) $\alpha=90°$.

defined by the angle δ shown in Fig. 8 is much less confined to small angles than in the previous case. This is due to a lower effective index of refraction and to the previously mentioned distribution of phase shifts.

C. Isotropic droplet with surface-induced nematic layer

There has been considerable interest over the last few years in the development of surface order in nematic liquid crystals.[15–20] Theoretical considerations show that near the N-I phase transition surface-induced nematic order can extend for several tenths of the (zero temperature) coherence length[18] (ξ_0) in the bulk isotropic liquid-crystal phase. For certain strengths of surface interactions, the surface phase transition is expected.[18,29] Here we are going to treat the effect of the radially oriented nematic layer, which is expected in the case of strong normal anchoring on the liquid-crystal–polymer surface. For the sake of simplicity, we assume the exponential decay of the nematic order parameter $s(r)=s(R)e^{-(R-r)/\xi_S}$, where $R \gg \xi_S \gg \xi_0$. The detailed treatment of the nematic-isotropic transition in a droplet with radial structure will be published elsewhere.[29] The description developed in Sec. IV B can be used here as well. We must substitute $n_0 \to n_0(r)$ and $n_e \to n_e(r)$, where

$$n_e(r)=\tfrac{1}{3}[n_e+2n_0+2(n_e-n_0)s(r)/s(R)]\ , \tag{48a}$$

$$n_0(r)=\tfrac{1}{3}[n_e+2n_0-(n_e-n_0)s(r)/s(R)]\ . \tag{48b}$$

Taking into account $r=\{r''^2+[\tfrac{1}{2}(R^2-r''^2)-l]^2\}^{1/2}$ and inserting Eq. (48) into Eqs. (23a) and (41b), one can follow the procedure in Sec. IV B and calculate the differential and the total cross sections for these cases. The total cross section presented in Fig. 12 for different ξ_S and $n_m=1.55$, $n_0=1.52$, and $n_e=1.70$, do not show any peculiarities. The case $\xi_S \to 0$ corresponds to the isotropic case with $n=(n_e+2n_0)/3$. To detect the surface-induced orders, one must choose $(n_e+2n_0)/3=n_m$. The resulting angular dependence (see Fig. 13) of the differential cross section ($kR=20$) has a very strong secondary maximum, which is expected to be observable even for thin surface layers.

V. CONCLUSIONS

We have presented, for the first time, a study of light scattering from supramicrometer-size birefringent nematic droplets embedded in a polymeric matrix. This study is a continuation of the work devoted to scattering from submicrometer droplets.[14] In common to both studies is the small difference of the indices of refraction of the

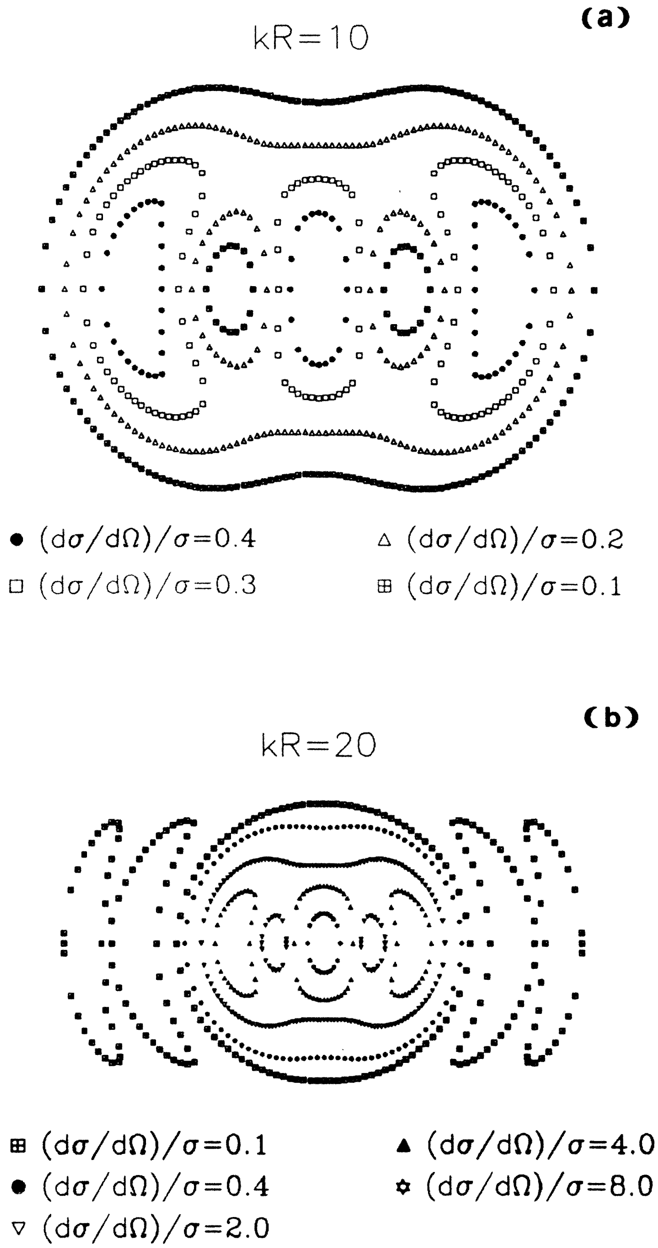

FIG. 11. Schematic presentation of the diffraction pattern (with lines of constant intensity); (a) for $kR=10$ and (b) for $kR=20$; $n_0=1.52$, $n_m=1.55$, and $n_e=1.70$ are used.

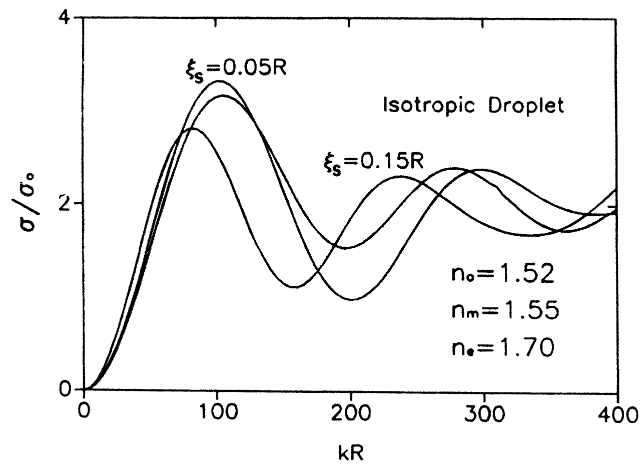

FIG. 12. The kR dependence of the total cross section of the isotropic droplet with a normally oriented nematic surface layer ($n_0=1.52$, $n_m=1.55$, and $n_e=1.70$) for two thicknesses. The isotropic case is presented as well.

This could help us better understand the effect of confinement on the nematic phase, the surface-induced ordering, and the possibility of the isotropic-nematic surface phase transition. The possibility of changing the internal structure either by application of an external field or by altering the temperature introduces numerous optoelectronic applications. Therefore our study can be used to optimize the scattering properties of nematic droplets important for optoelectronic devices.

liquid crystal and polymer. Therefore, we were able to use the Rayleigh-Gans approach for submicrometer droplets and in this paper the anomalous-diffraction approach for supramicrometer-size droplets. The scattering patterns are shown to exhibit strong dependencies on the different director configurations; therefore, experimental study of the light scattering can be a powerful tool in determining the details of the nematic-director configuration in the droplet for a carefully chosen droplet size and value of the index of the refraction of the matrix.

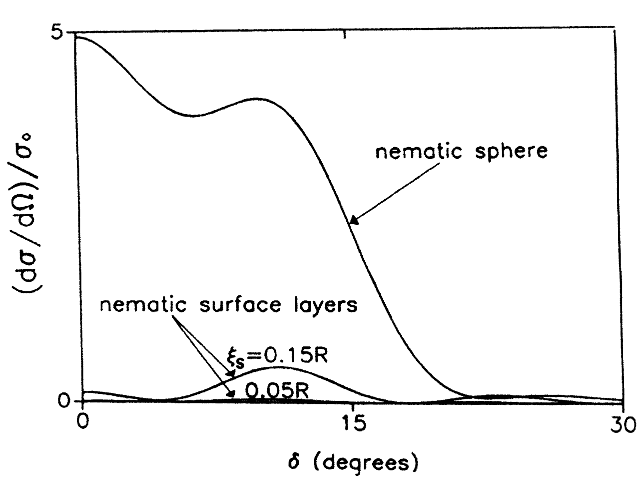

FIG. 13. The angular dependence of the differential cross section of the isotropic droplet with a normally oriented nematic surface layer for two thicknesses ($n_0=n_m=1.52$ and $n_e=1.70$). The case of the nematic droplet is shown as well.

ACKNOWLEDGMENTS

Support for this research by the General Motors Research Laboratories and the National Science Foundation, Solid-State Chemistry, Grant No. DMR85-03219, is acknowledged. The author acknowledges Professor J. W. Doane for stimulating discussions. The computer calculations were performed by Gregory Crawford.

*Permanent address: Department of Physics, E. Kardelj University of Ljubljana, Jadranska 19, 61000 Ljubljana, Yugoslavia.

[1]M. Kerker, *The Scattering of Light and Other Electromagnetic Radiation* (Academic, New York, 1969).

[2]C. F. Bohren and D. R. Hoffman, *Absorption and Scattering of Light by Small Particles* (Wiley, New York, 1983).

[3]I. O. Kulik and A. G. Shkorbatov, Opt. Spektrosk. **51**, 701 (1981) [Opt. Spectrosc. (USSR) **51**, 389 (1981)].

[4]J. Roth and M. J. Digmen, J. Opt. Soc. Am. **63**, 308 (1973).

[5]R. S. Stein and M. B. Rhodes, J. Appl. Phys. **13**, 1873 (1960).

[6]M. B. Rhodes and R. S. Stein, J. Polym. Sci. A **2**, 1539 (1969).

[7]J. V. Champion, A. Killey, and G. H. Meeten, J. Polym. Sci. Polym. Phys. Ed. **23**, 1467 (1985).

[8]Lord Rayleigh, Philos. Mag. **41**, 107 (1871); **41**, 274 (1871); **41**, 447 (1871).

[9]R. Gans, Ann. Phys. (Leipzig) **76**, 29 (1925).

[10]H. C. van de Hulst, Physics (N.Y.) **15**, 740 (1949).

[11]H. C. van de Hulst, *Light Scattering by Small Particles* (Wiley, New York, 1957).

[12]J. W. Doane, N. A. Vaz, B.-G. Wu, and S. Žumer, Appl. Phys. Lett. **48**, 4 (1986).

[13]J. Fergason, SID J. **16**, 68 (1985).

[14]S. Žumer and J. W. Doane, Phys. Rev. A **34**, 3373 (1986).

[15]H. Schröder, J. Chem. Phys. **67**, 16 (1977).

[16]K. Miyano, J. Chem. Phys. **71**, 4108 (1979).

[17]D. W. Allender, G. L. Henderson, and D. L. Johnson, Phys. Rev. A **25**, 1086 (1981).

[18]P. Sheng, Phys. Rev. A **26**, 1610 (1982).

[19]T. J. Sluckin and A. Poniewierski, Phys. Rev. Lett. **55**, 2907 (1985).

[20]A. K. Sen and D. E. Sullivan, Phys. Rev. A **35**, 1391 (1987).

[21]M. Born and E. Wolff, *Principles of Optics* (Pergamon, London, 1980).

[22]E. Dubois-Violette and O. Parodi, J. Phys. C **4**, 57 (1969).

[23]R. D. Williams, J. Phys. A **19**, 3211 (1986).

[24]P. Sheng, Phys. Rev. A **26**, 1610 (1982).

[25]J. W. Allender and S. Žumer, Bull. Am. Phys. Soc. **31**, 691 (1986).

[26]A. J. Nicastro and P. H. Keyes, Phys. Rev. **30**, 3156 (1984).

[27]P. G. de Gennes, *The Physics of Liquid Crystals* (Clarendon, Oxford, 1974).

[28]W. F. Ames, *Numerical Methods for Partial Differential Equations* (Academic, New York, 1977).

[29]S. Žumer and D. W. Allender (unpublished).